Project Acronym:

BRAINSONIC (ENTERPRISES/0223/Sub-Call1/0057)

MRI-guided Focused Ultrasound robotic system for brain tumors.

Deliverable number: 5.1

Title: MRI compatibility and motion accuracy of the robotic system.

Prepared by:

Anastasia Antoniou (CUT)
Nikolas Evripidou (CUT)
Christakis Damianou (CUT)

Date: 02/07/2025

Funded by the European Union NextGenerationEU

Cyprus tomorrow RECOVERY AND RESILIENCE PLAN

Republic of Cyprus

RESEARCH & INNOVATION FOUNDATION

The BRAINSONIC project is funded by the Recovery and Resilience Facility of the NextGenerationEU instrument, through the Research and Innovation Foundation (RIF) of Cyprus.

Contents

EXECUTIVE SUMMARY

This deliverable describes the procedures implemented to assess the compatibility of the developed BRAINSONIC robotic system with a high field Magnetic Resonance Imaging (MRI) scanner, as well as the accuracy and repeatability of robotic motion. The relevant methodologies employed and obtained results are presented in detail.

For MRI compatibility assessment, two main MRI sequences were employed, namely T2-Weighted (T2-W) Turbo Spin Echo (TSE) and Spoiled Gradient (SPGR) sequences. Images of an agar-based homogeneous MRI phantom were acquired under different activation conditions of the electronic system and amplifier and compared in terms of Signal-to-Noise ratio (SNR) and overall quality. Since the robotic system comprises components that require electricity to operate (e.g., motors and encoders), it is classified as MRI-conditional as per American Society for Testing and Materials (ASTM) standards (F2503, F2052, F2213, F2182, and F2119) for medical devices in MRI.

A simple and straightforward method involving the use of a digital calliper was employed to evaluate the inherent accuracy and repeatability of robotic motion in the laboratory setting. In brief, the accuracy of linear motion in all axes (X, Y, Z) was tested using a digital caliper and 3D-printed holders that were specially designed to facilitate proper attachment of the caliper on the three motion stages. The ability of the robot to move and execute specific motion commands with the required precision and accuracy was evaluated by comparing the intended and actual movements. As part of this experiment, the motion speed in each axis was also estimated based on the motors' activation time needed to cover specific distances.

After laboratory validation, the system underwent testing in the MRI setting that more accurately reflects realistic conditions, accounting for any additional errors that may arise, potentially due to magnetic interference. The specific purpose was to measure the linear motion accuracy of the device through high-resolution imaging. Specifically, the methodology entailed comparing a series of Fast Low Angle Shot (FLASH) images of a plastic marker; serving as the end effector of the mechanism, sequentially acquired after execution of repetitive 3-mm step movements in each orthogonal axis (X, Y, Z).

1. Assessment of MRI compatibility

1.1 Materials and Methods

The BRAINSONIC system incorporates a single element spherically focused transducer (Frequency = 2.6 MHz; Diameter = 50 mm; Radius of curvature = 65 mm; Efficiency = 30 %) that can be moved in three linear (X, Y, Z) and one angular axes. For the MRI experiments reported herein, the transducer was driven by an AG1016 RF amplifier (AG Series Amplifier, T & C Power Conversion, Inc., Rochester, USA), located outside of the MRI room. The system also comprises a custom-made electronic driving system that controls the ultrasonic motors and encoders, which was also situated outside of the MRI room and connected with the device through specially shielded cables. The system was assessed for MRI compatibility in a 3T MRI scanner (Magnetom Vida, Siemens Healthineers, Erlangen, Germany) by examining the effect of different activations of the amplifier/transducer and electronic system on the imaging quality.

The SNR served as the main metric for the quantitative assessment of the MRI compatibility. The relevant experimental setup as arranged on the MRI table can be seen in **Figure 1**. The device was positioned on the patient couch and an agar-based phantom with a 6% weight per volume (w/v) agar concentration was placed on its acoustic opening. The coil (Ultraflex 18 Large, Siemens Healthineers) was positioned in close proximity above the phantom using a dedicated 3D printed holder.

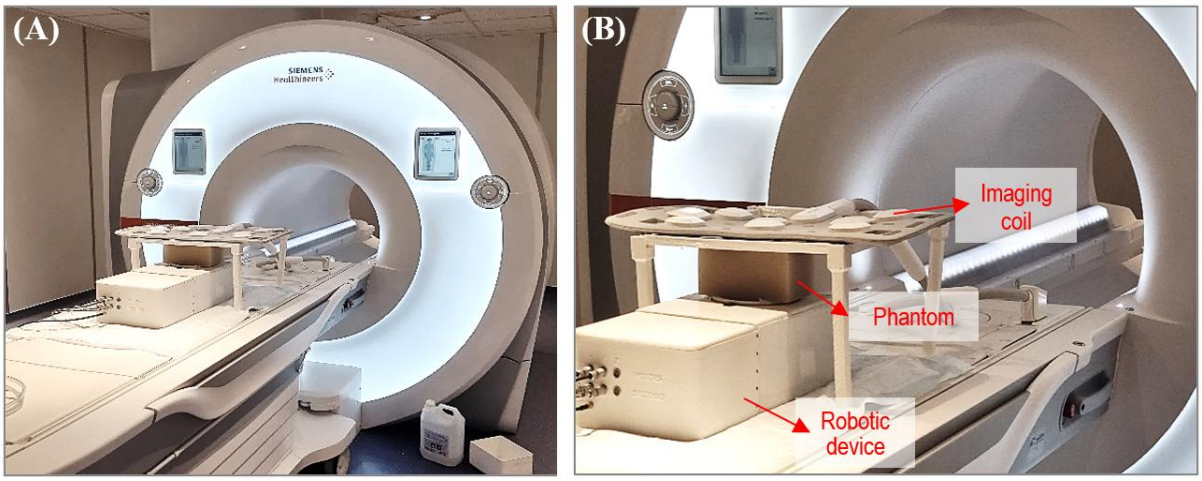

***Figure 1**: (A) Experimental set-up inside the 3T MRI scanner with the robotic device seated on the table with an agar phantom placed on its acoustic window. (B) Closer view with main components indicated.*

The phantom was scanned using 2D Spoiled Gradient Echo (SPGR) and T2-Weighted (T2-W) Turbo Spin Echo (TSE) sequences. The SNR was calculated by the mean signal intensity measured in a single Region of Interest (ROI) set within the phantom (SI_{tissue}) relative to the standard deviation of the SI measured within a similar ROI set in the background; air (σ_{noise}) according to Equation 1:

$$SNR = {SI_{tissue}}/{\sigma_{noise}} \quad (1)$$

A series of 2D coronal and axial SPGR and T2-W TSE images of the phantom were acquired under the following activation states of the electronic system and amplifier:

1. Reference: NO cables connected.
2. Motor cables connected – DC OFF.
3. Motor cables connected – DC ON.
4. Motor cables connected – DC ON – X-axis moving.
5. Transducer cables connected – Amplifier OFF.
6. Transducer cables connected – Amplifier ON.
7. Transducer cables connected – Amplifier ON – RF power ON at 50 W.
8. ALL cables connected – DC OFF – Amplifier OFF.
9. ALL cables connected – DC ON – Amplifier OFF.
10. ALL cables connected – DC ON – Amplifier ON.
11. ALL cables connected – DC ON – Amplifier ON – RF power ON at 50 W.

The specific parameters employed for SPGR and T2-W TSE imaging, including the repetition time (TR), echo time (TE), flip angle (FA), number of averages (NEX), field of view (FOV), echo train length (ETL), matrix size, and pixel bandwidth (pBW) are listed in **Table 1** and **Table 2**, respectively.

Table 1: *SPGR sequence parameters for MRI compatibility assessment.*

Sequence name	**TR (ms)**	**TE (ms)**	**FA (°)**	**NEX**	**Transmit Coil Type**
***fl2d1**	25	10	30	1	Body
Slice thickness (mm)	**Matrix**	**pBW (Hz/Pixel)**	**FOV (mm^2)**	**ETL**	**Receive Coil Type**
6	96 x 96	250	280×280	1	Ultraflex 18 large Spine_72_RS

Table 2: *T2-W TSE sequence parameters for MRI compatibility assessment.*

Sequence name	**TR (ms)**	**TE (ms)**	**FA (°)**	**NEX**	**Transmit Coil Type**
***tseR2d1_30**	2000	52	110°	1	Body
Slice thickness (mm)	**Matrix**	**pBW (Hz/Pixel)**	**FOV (mm^2)**	**ETL**	**Receive Coil Type**
3	256 x 256	250	260 x 260	30	Ultraflex 18 large Spine_72_RS

1.2 Results

Figure 2 shows the acquired coronal SPGR magnitude images of the phantom for the various activation states tested, while the relevant SNR measurements are displayed in the bar chart of **Figure 3**. **Figure 4** shows the corresponding coronal SPGR phase images. For the axial plane, the results are presented in **Figure 5 to Figure 7**.

Figure 8 and **Figure 9** display the series of T2-W magnitude images of the phantom acquired in coronal plane and corresponding SNR measurements in the form of a bar chart, respectively. Similarly, **Figure 10** and **Figure 11** present the results obtained for the axial plane.

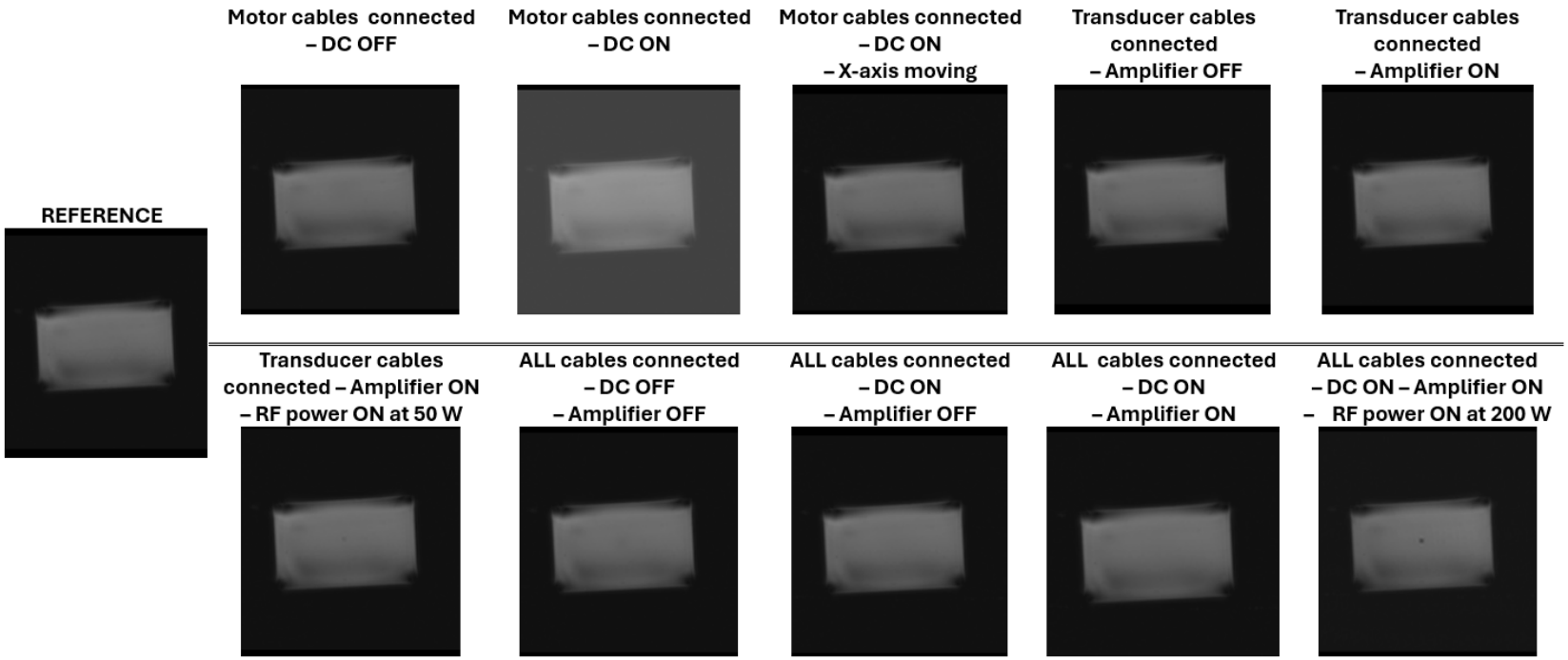

***Figure 2**: Coronal 2D SPGR magnitude images acquired under different activation conditions of the BRAINSONIC system.*

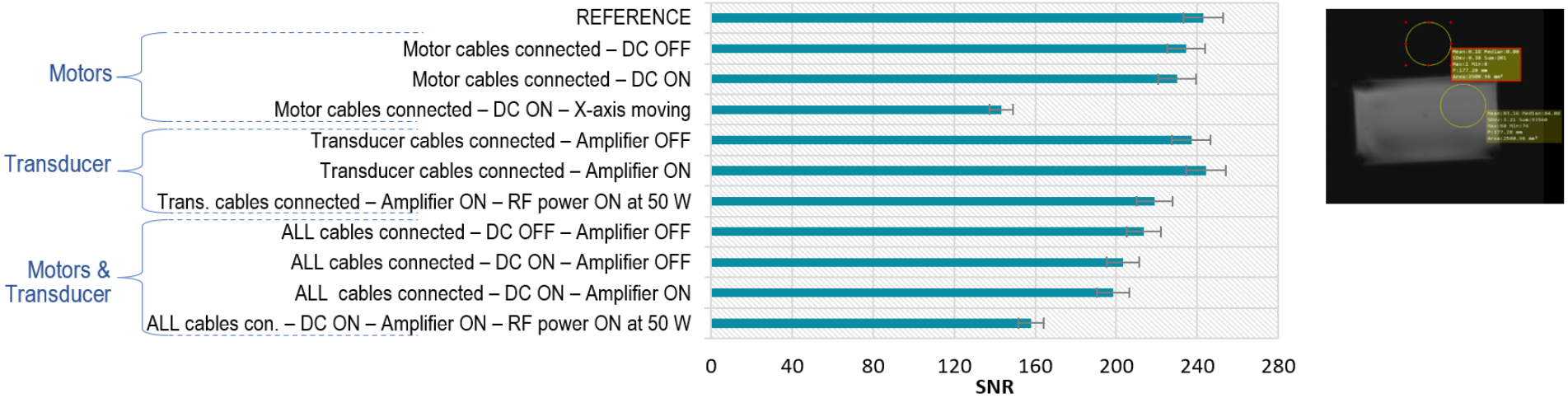

***Figure 3**: Bar chart of the corresponding SNR values calculated for the different activation conditions (from coronal SPGR images).*

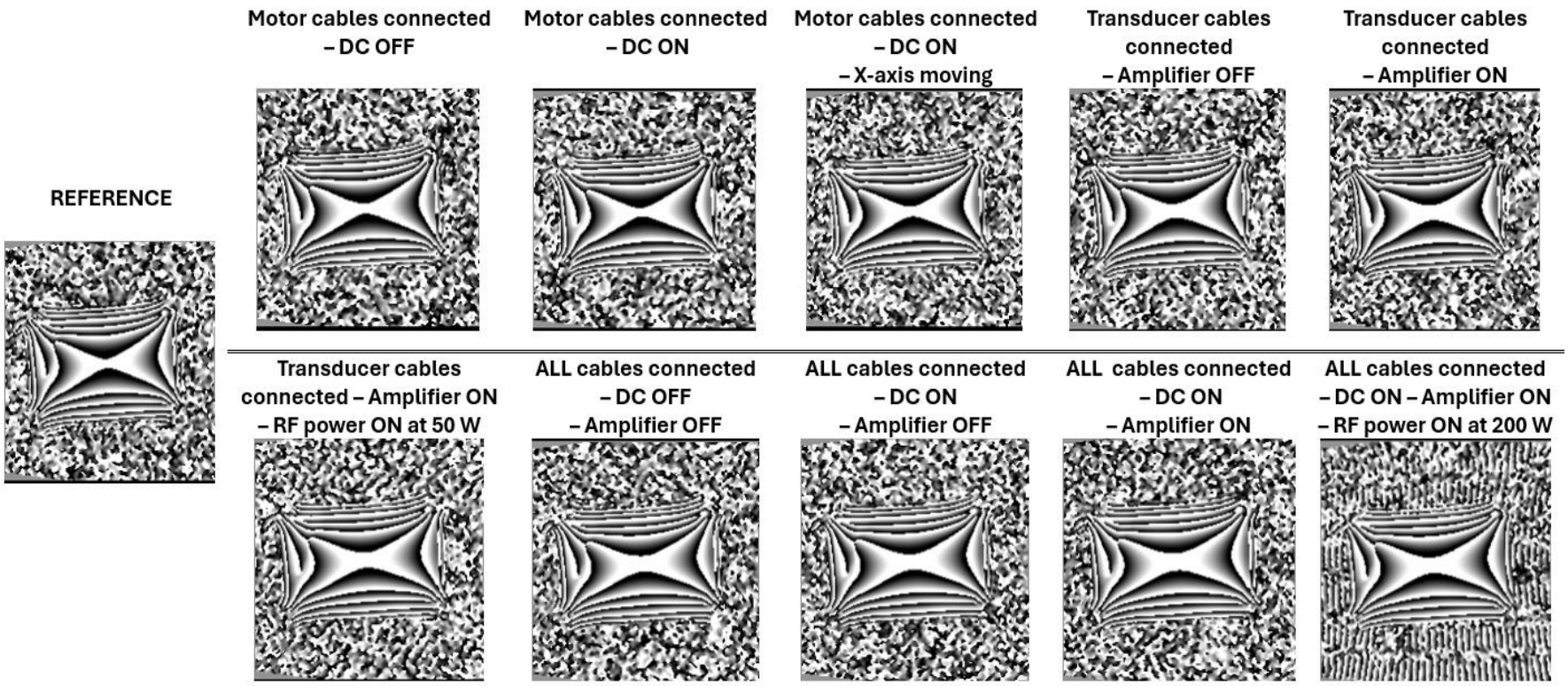

Figure 4*: Coronal 2D SPGR phase images acquired under different activation conditions of the BRAINSONIC system.*

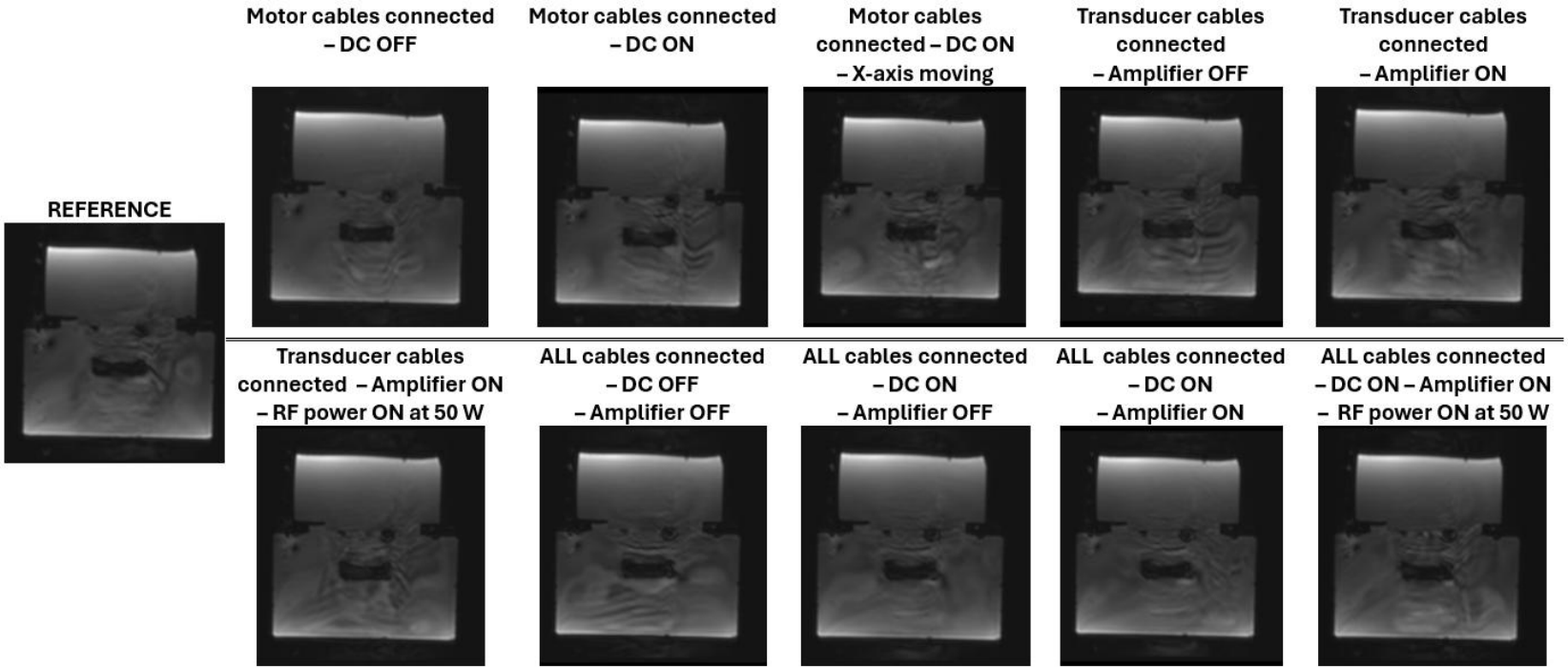

***Figure 5**: Axial 2D SPGR magnitude images acquired under different activation conditions of the BRAINSONIC system.*

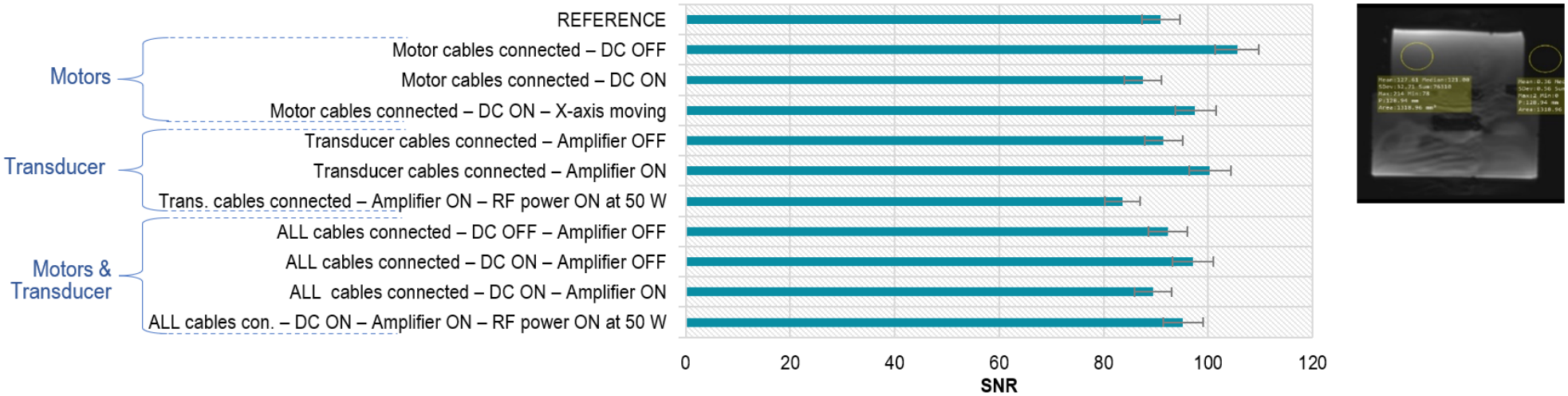

***Figure 6**: Bar chart of the corresponding SNR values calculated for the different activation conditions (from axial SPGR images).*

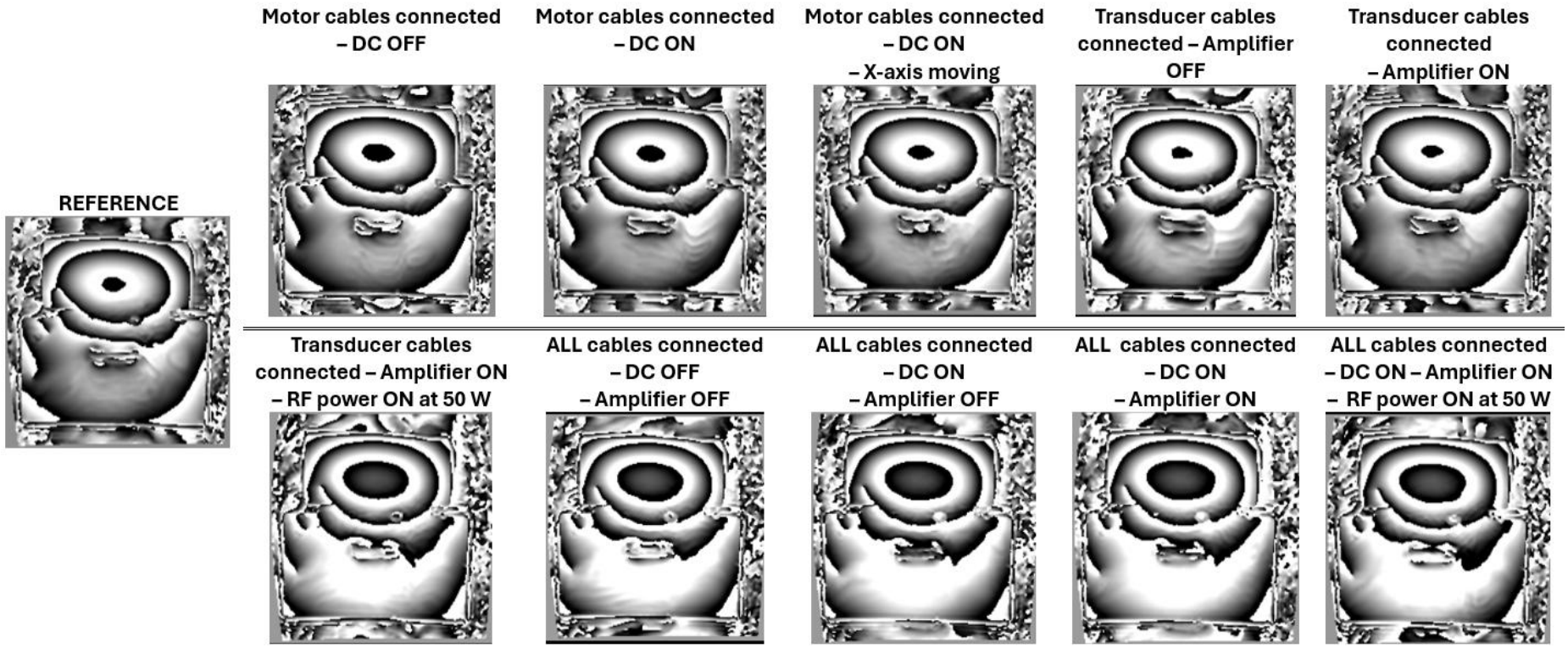

***Figure** 7: Axial 2D SPGR phase images acquired under different activation conditions of the BRAINSONIC system.*

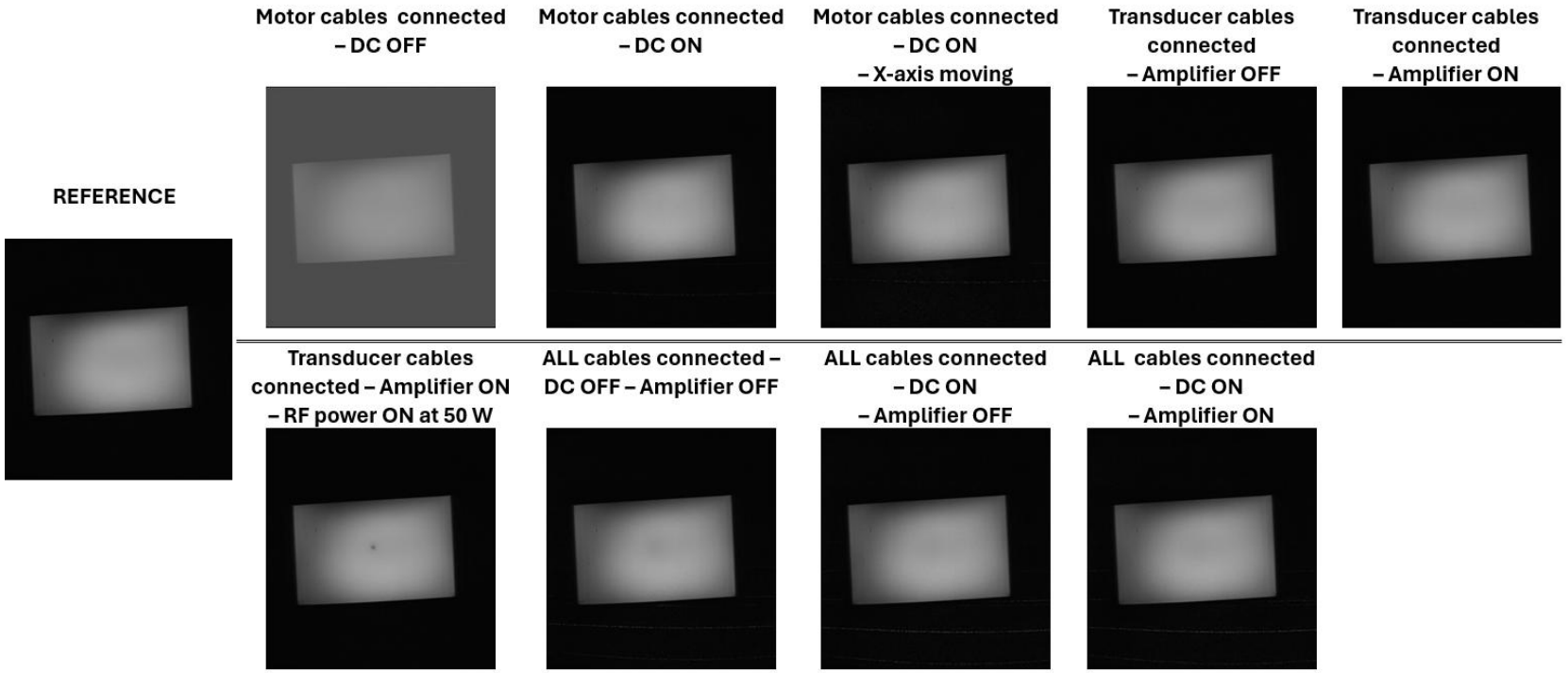

Figure 8: *Coronal 2D T2-W magnitude images acquired under different activation conditions of the BRAINSONIC system.*

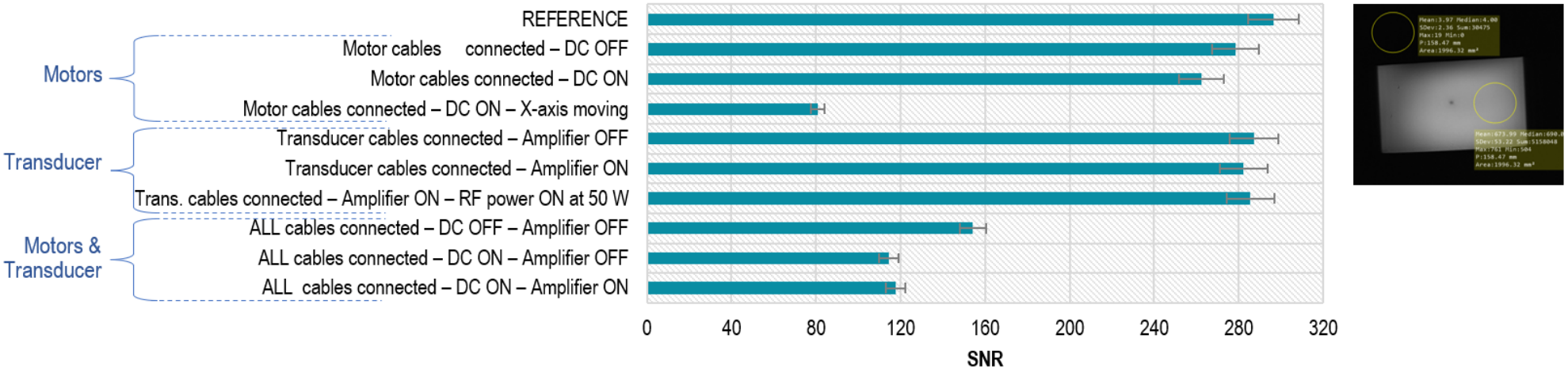

Figure 9: *Bar chart of the corresponding SNR values calculated for the different activation conditions (from coronal T2-W images).*

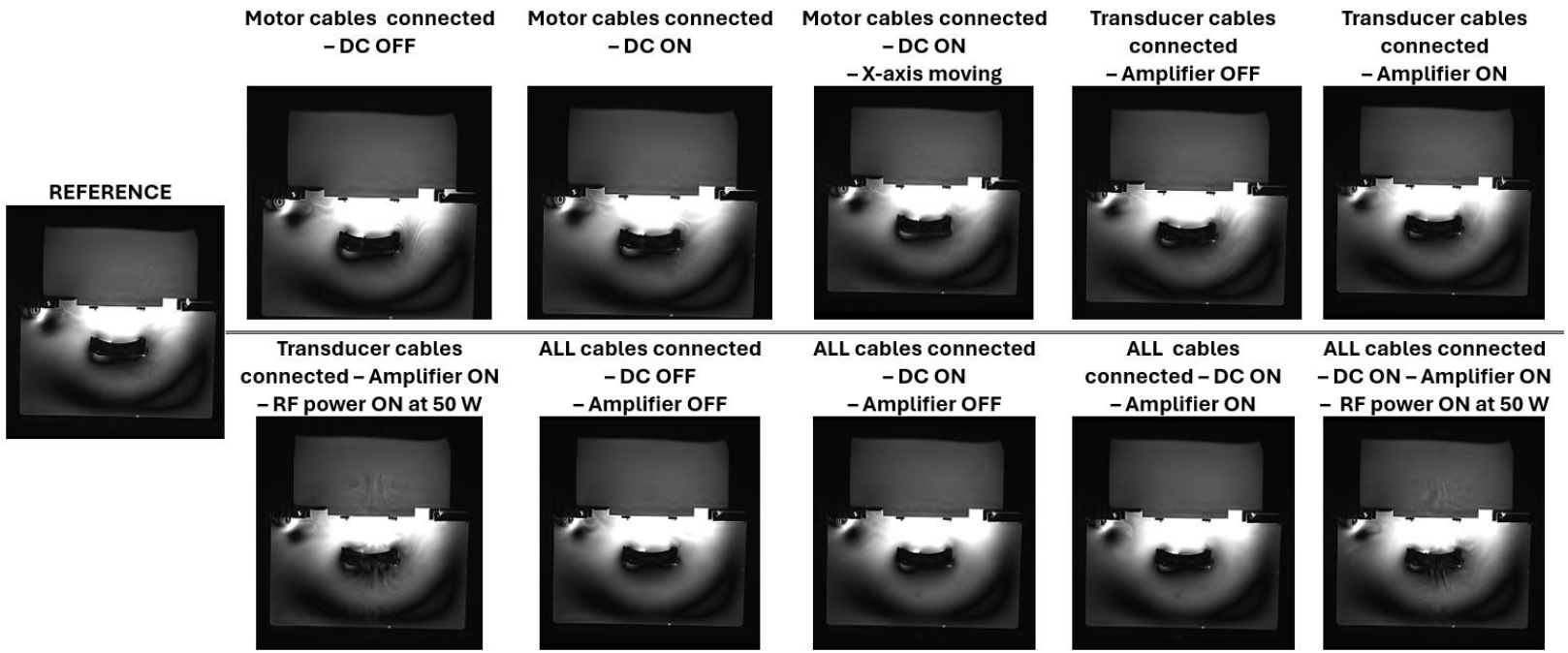

***Figure 10**: Axial 2D T2-W magnitude images acquired under different activation conditions of the BRAINSONIC system.*

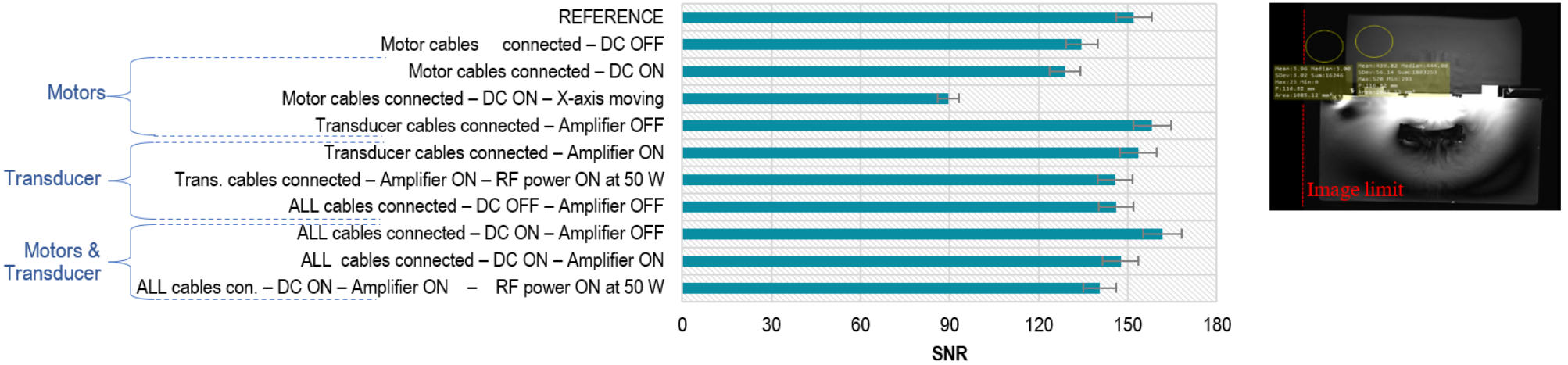

***Figure 11**: Bar chart of the corresponding SNR values calculated for the different activation conditions (from axial T2-W images).*

1.3 Interpretation of Results

Coronal SPGR imaging:
Regarding activation of the electronic system, a significant SNR drop was observed upon initiation of motion in the X-axis (about 40% reduction). Turning on the amplifier did not decrease the reference SNR but initiating sonication at 50 W reduced slightly the SNR by 10%. Connecting all cables resulted in a similar reduction in SNR (approximately 12%), which was further decreased gradually by turning on the DC switch, followed by activating the amplifier, and finally initiating sonication (50 W). This eventually led to a total SNR reduction of 35% compared to the original level (Figure 3). There were no (visible) artifacts present on the images (Figure 2). This was confirmed by visual inspection of phase images (Figure 4), which maintained consistent quality across the different activation states of the robot. By consistent quality we mean that the images exhibited similar characteristics without significant variations in visual features (brightness, contrast, geometry) or distortions.

Axial SPGR imaging:
The images acquired in the axial plane did not exhibit any specific pattern among activation states in terms of the acquired SNR. Surprisingly, neither the initiation of motion in the X-axis nor sonication (with all cables connected) led to a decrease in SNR; instead, a slight increase was observed compared to the reference value. These random SNR variations, reaching up to 15% (Figure 6), may be attributed to the presence of the transducer within the field of view in the axial plane, potentially introducing susceptibility artifacts. These artifacts may have influenced the SNR measurements, unavoidably complicating the interpretation of the results. Across all axial SPGR images of the imaged phantom (Figure 5), a slight distortion is consistently observed within the phantom (right side). The corresponding phase images exhibited noticeable alterations in phase contrast patterns (Figure 7).

T2-W imaging:
In the axial T2-W images, the SNR gradually decreased from the reference value of 152 to about 90 when transitioning from the 'Motor cables connected – DC OFF' state to 'Motor cables connected - DC ON' and then 'X-axis moving' states (Figure 11). In the coronal plane, a larger SNR drop was observed with the reference value of 297 decreasing to 81 (Figure 9). Connection of transducer cables and sonication at 50 W resulted in only about 4% decrease in the SNR of both axial and coronal T2-W images. Visually, the acquired T2-W images (Figure 8 and Figure 10) did not exhibit noticeable differences between them. As expected, some distortion was observed at the centre of the phantom under the 'RF power on' state due to the sonication (Figure 10). Also note that during sonication the heated region appeared as a spot of reduced intensity in coronal T2-W images.

2. Assessment of motion accuracy in laboratory setting

2.1 Materials and Methods

The purpose of this section was to assess the linear motion accuracy of the BRAINSONIC robotic system utilizing a digital caliper in a laboratory setting.

2.1.1 Motion accuracy

The accuracy and repeatability of motion in each of the three orthogonal axes (X, Y, Z) was assessed utilizing a digital caliper (ROHS NORM 2002/95/EC) and dedicated 3D-printed holders. These holders were produced on a 3D printer (FDM 270, Stratasys, Minnesota, USA) with Acrylonitrile styrene acrylate (ASA) thermoplastic. They were fixed on the motion stages to align the digital caliper with the relevant axes and facilitate precise measurements. An indicative photo of the experimental setup used for measurements along the Y-axis can be seen in **Figure 12. Figure 13** is a closer view of the setup showing the caliper as integrated on the evaluated motion stage.

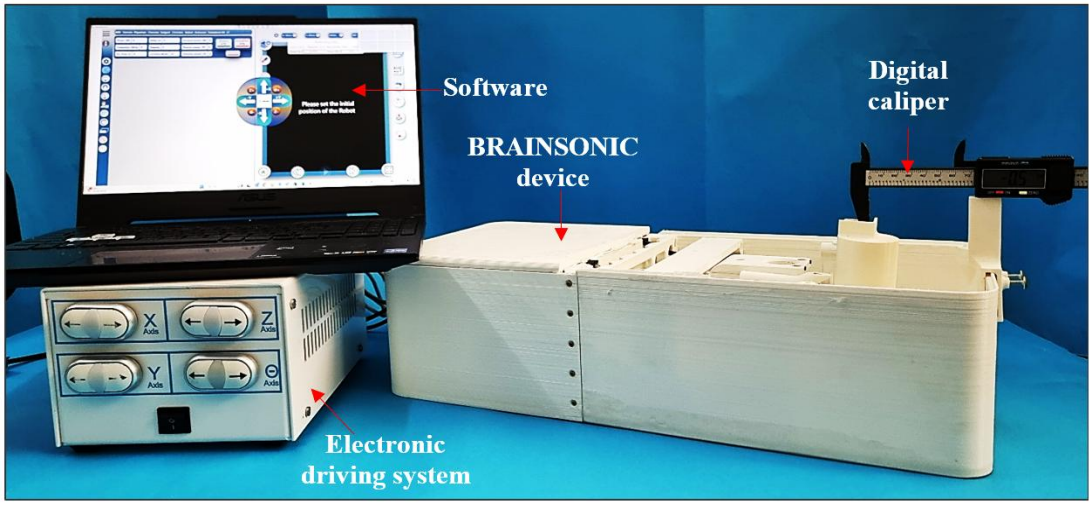

***Figure 12**: Experimental set-up for linear motion accuracy assessment in the laboratory.*

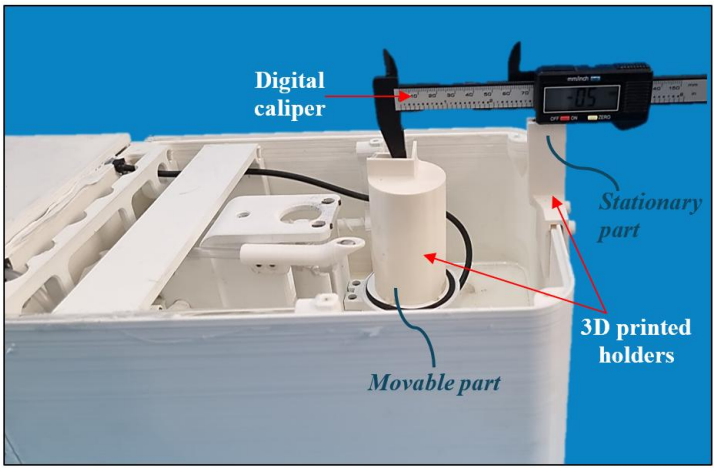

***Figure 13**: Closer view of the experimental setup showing the caliper as integrated on the Y-stage for motion accuracy assessment.*

The accuracy of motion was defined as the robot's ability to move specific distances and was assessed in both directions of each linear axis. Each motion stage was commanded to repetitively move by 1, 3, 5, and 10 mm using the software's motion commands. The relevant actual displacements were recorded by the digital caliper.

2.1.2 Speed of motion

The speed of motion was estimated based on the time needed for the motion stages to cover a specific distance, which equals the duration of motor activation during execution of the relevant motion command, as measured by the Arduino microcontroller of the electronic system. Accordingly, the speed of motion in each axis was simply calculated by dividing the covered distance with the relevant recorded time. Step movements of 10 mm were repetitively performed (n=10) for motion speed calculation.

2.2 Results

2.2.1 Motion along the Y-axis

The point charts of **Figure 14 to Figure 17** display the measured displacement for each repetition (n=10) for bidirectional movements (right and left) of 1, 3, 5, and 10 mm in the Y-axis, respectively. **Figure 18** summarizes the accuracy results for the Y-axis motion in the form of a bar chart of the intended distance versus the mean actual distance as measured by the digital caliper.

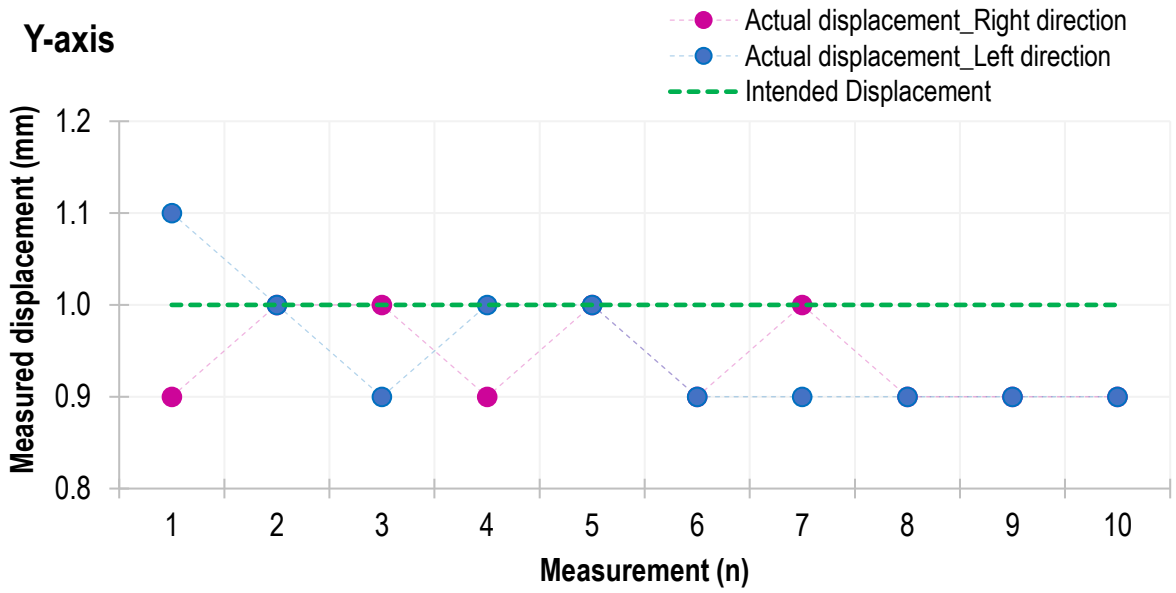

Figure 14: *Actual displacement measured for 1-mm step movement in the Y-axis right and left directions versus repetition (n=10). The dotted green line indicates the intended displacement.*

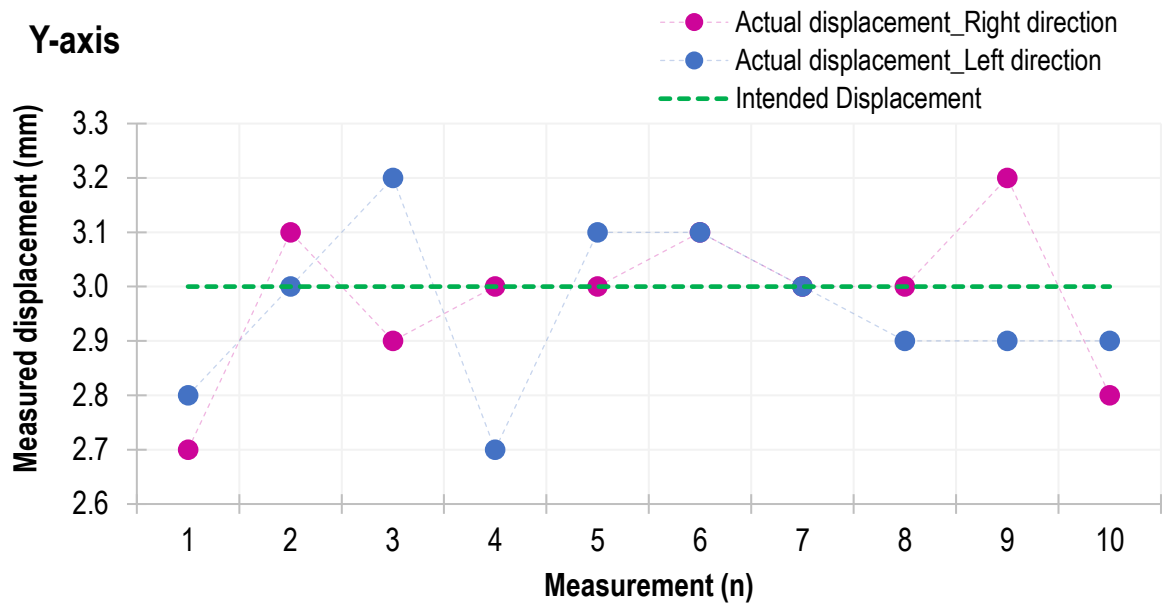

Figure 15: *Actual displacement measured for 3-mm step movement in the Y-axis right and left directions versus repetition (n=10). The dotted green line indicates the intended displacement.*

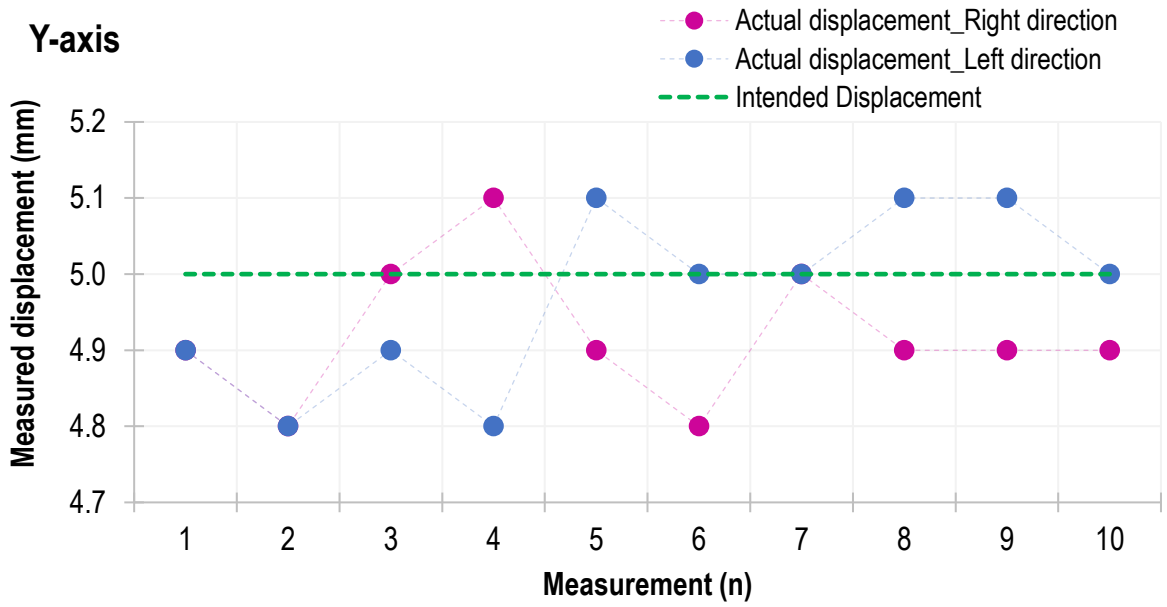

Figure 16: *Actual displacement measured for 5-mm step movement in the Y-axis right and left directions versus repetition (n=10). The dotted green line indicates the intended displacement.*

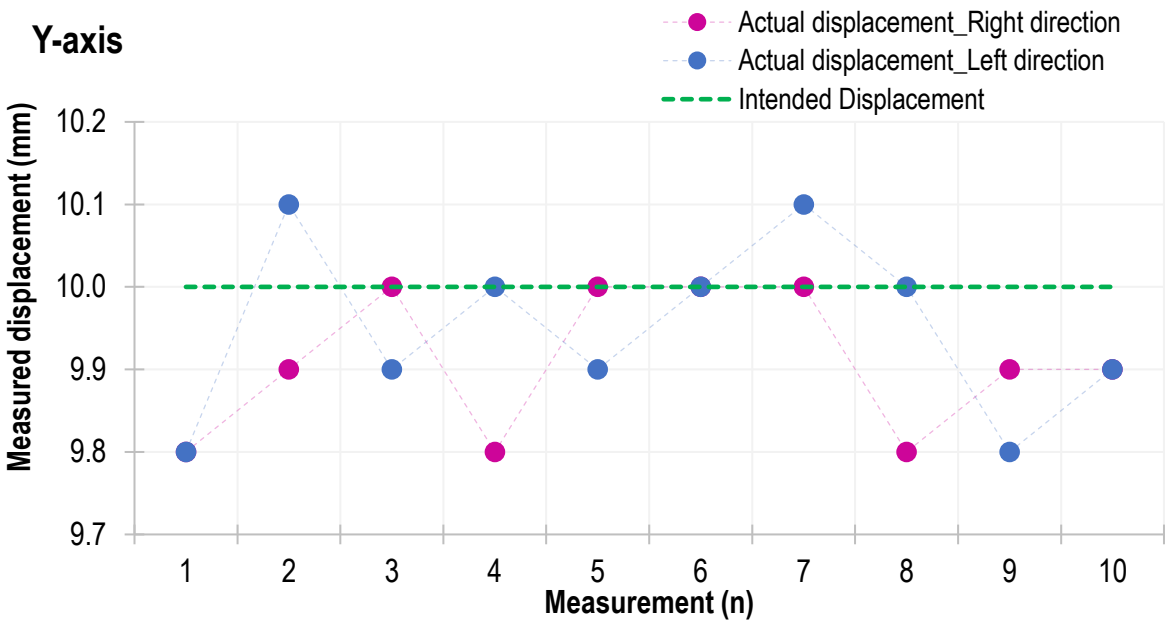

Figure 17: *Actual displacement measured for 10-mm step movement in the Y-axis right and left directions versus repetition (n=10). The dotted green line indicates the intended displacement*

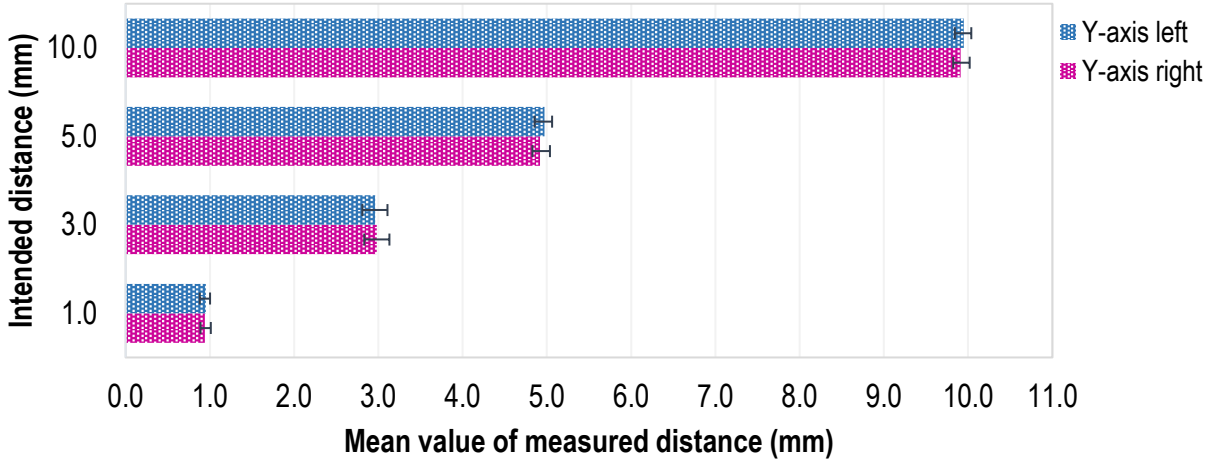

Figure 18*: Intended distance versus mean value of measured distance in the Y-axis right and left directions. Error bars represent the standard deviation of the mean.*

2.2.2 Motion along the X-axis

The point charts of **Figure 19 to Figure 22** display the measured displacement for each repetition (n=10) for bidirectional movements (forward and reverse) of 1, 3, 5, and 10 mm in the X-axis, respectively. **Figure 23** summarizes the accuracy results for the X-axis motion in the form of a bar chart of the intended distance versus the mean actual distance as measured by the digital caliper.

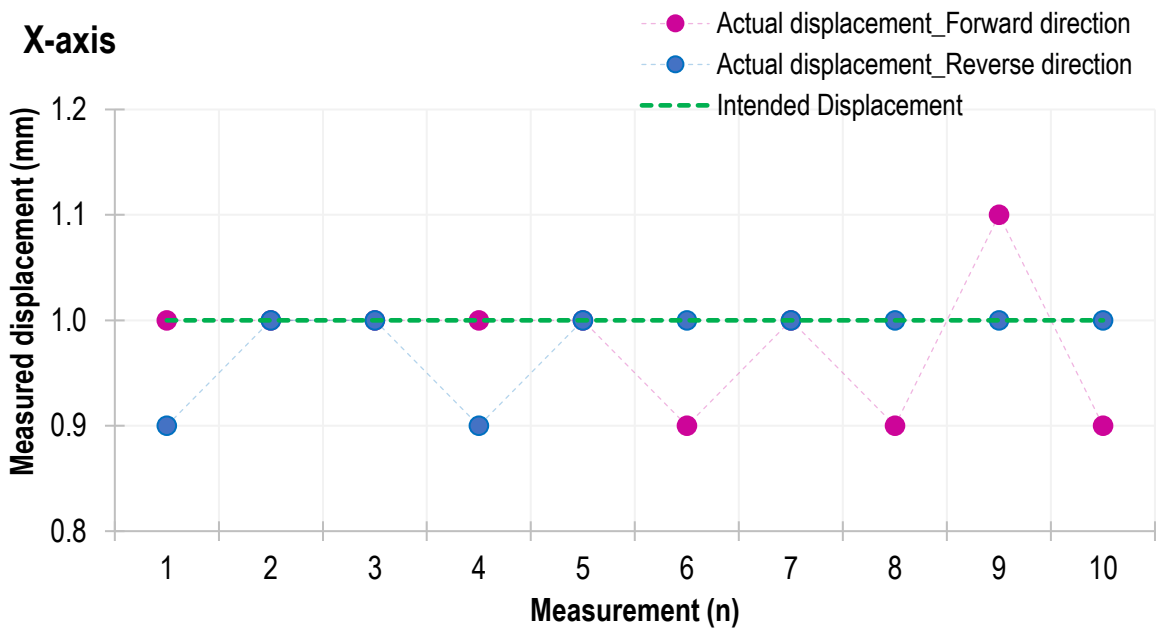

Figure 19: *Actual displacement measured for 1-mm step movement in the X-axis forward and reverse directions versus repetition (n=10). The dotted green line indicates the intended displacement.*

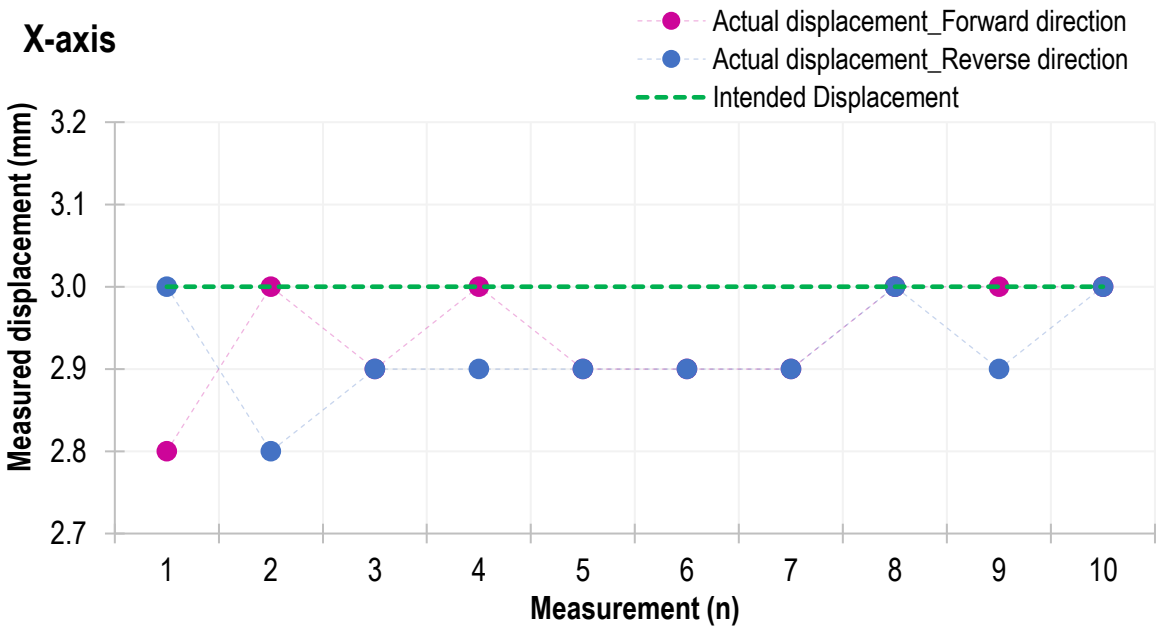

Figure 20: *Actual displacement measured for 3-mm step movement in the X-axis forward and reverse directions versus repetition (n=10). The dotted green line indicates the intended displacement.*

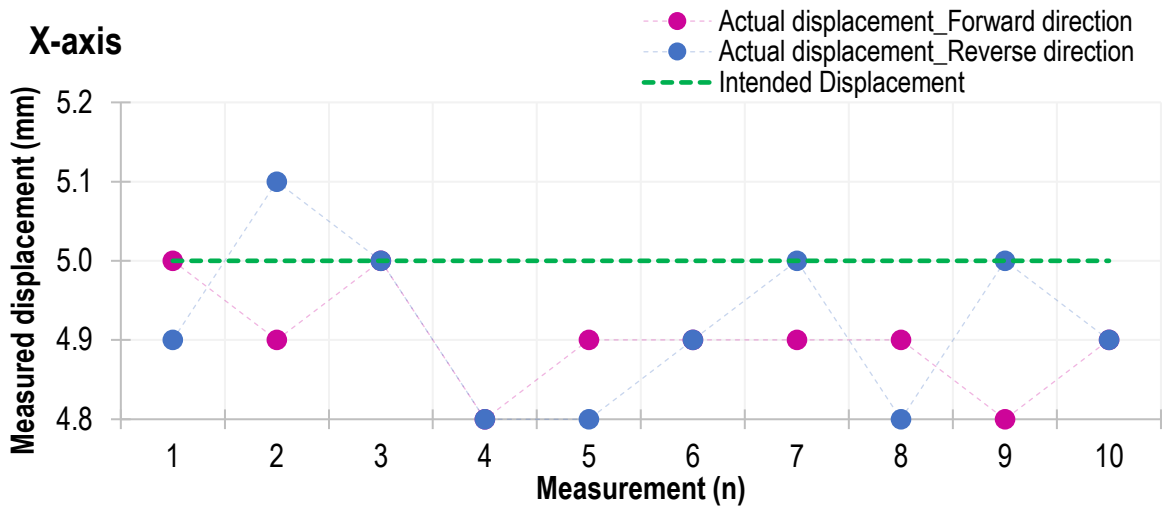

Figure 21: *Actual displacement measured for 5-mm step movement in the X-axis forward and reverse directions versus repetition (n=10). The dotted green line indicates the intended displacement.*

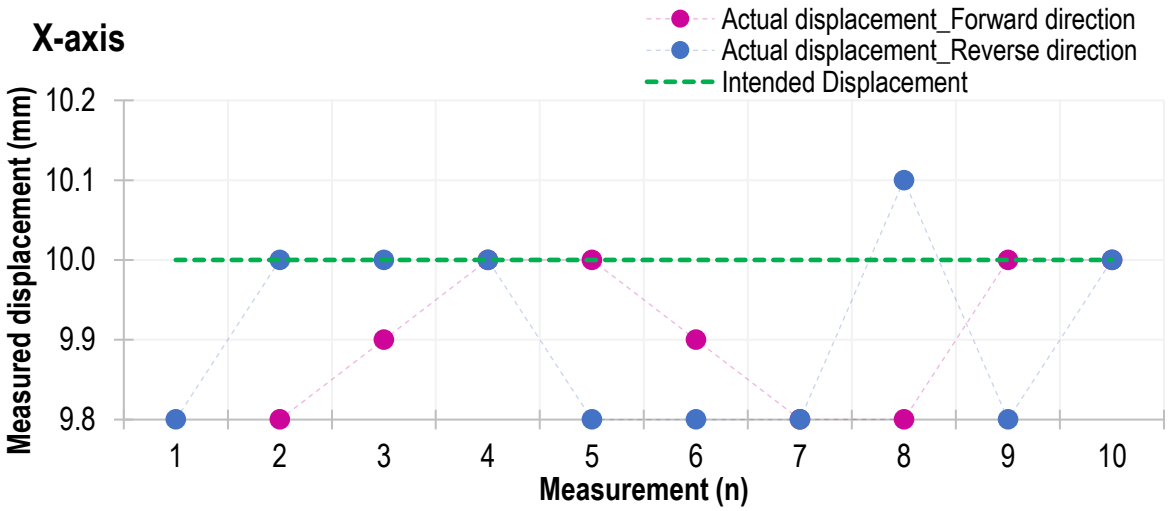

Figure 22: *Actual displacement measured for 10-mm step movement in the X-axis forward and reverse directions versus repetition (n=10). The dotted green line indicates the intended displacement.*

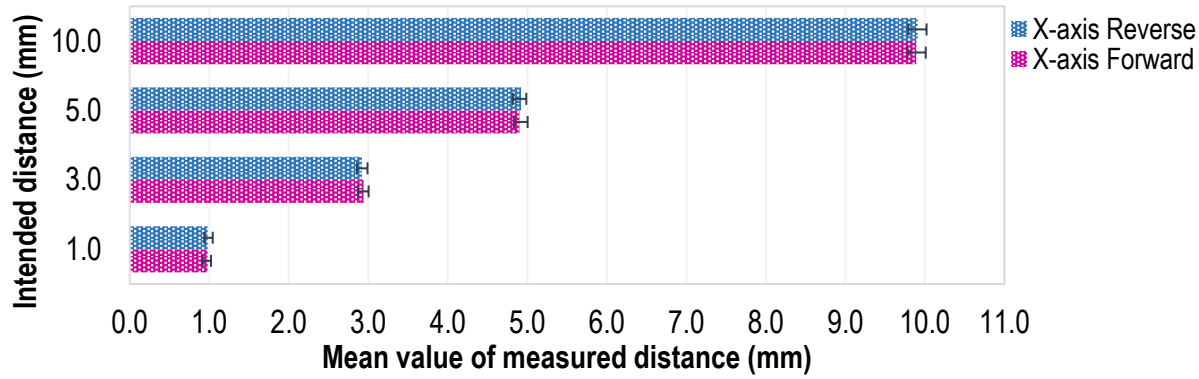

Figure 23*: Intended distance versus mean value of measured distance in the X-axis forward and reverse directions. Error bars represent the standard deviation of the mean.*

2.2.3 Motion along the Z-axis

The point charts of **Figure 24 to Figure 27** display the measured displacement for each repetition (n=10) for bidirectional movements (upward and downward) of 1, 3, 5, and 10 mm in the Z-axis, respectively. **Figure 28** summarizes the accuracy results for the Z-axis motion in the form of a bar chart of the intended distance versus the mean actual distance as measured by the digital caliper.

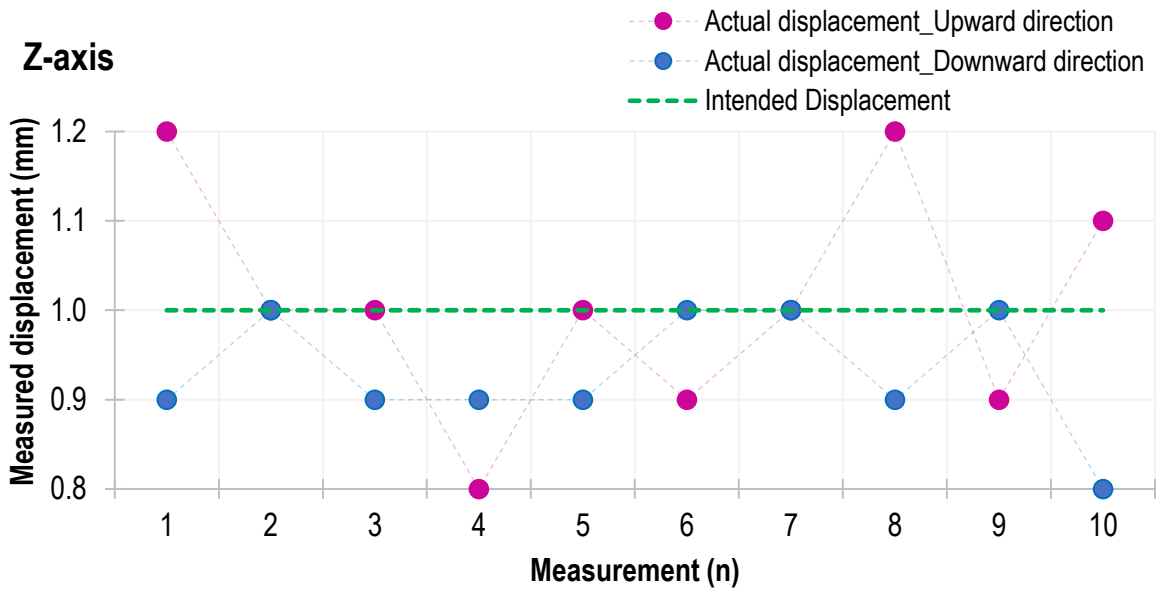

Figure 24: *Actual displacement measured for 1-mm step movement in the Z-axis upward and downward directions versus repetition (n=10). The dotted green line indicates the intended displacement.*

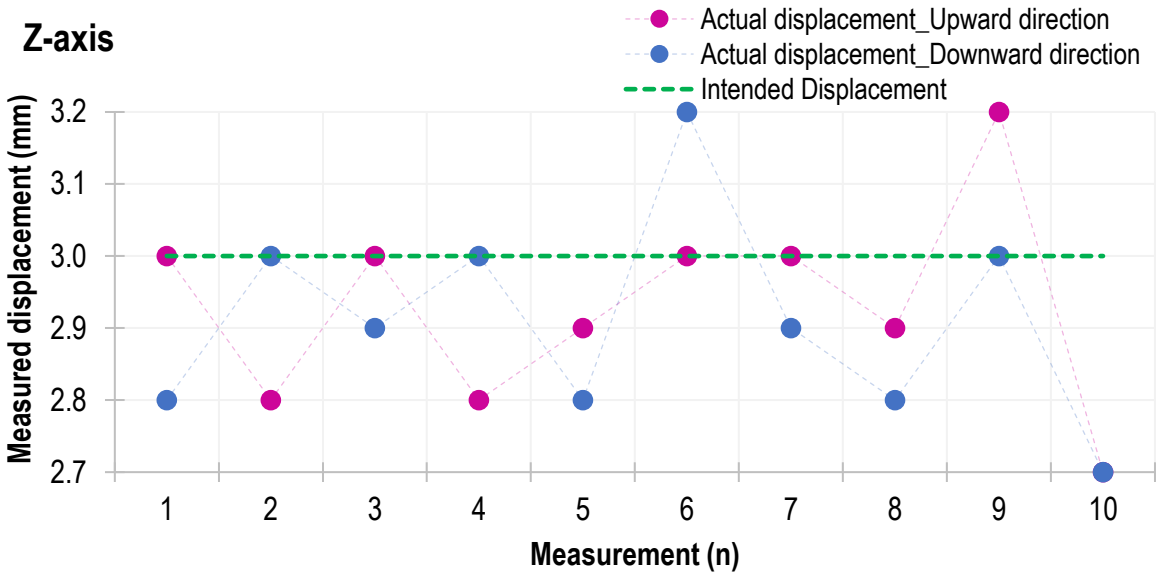

Figure 25: *Actual displacement measured for 3-mm step movement in the Z-axis upward and downward directions versus repetition (n=10). The dotted green line indicates the intended displacement.*

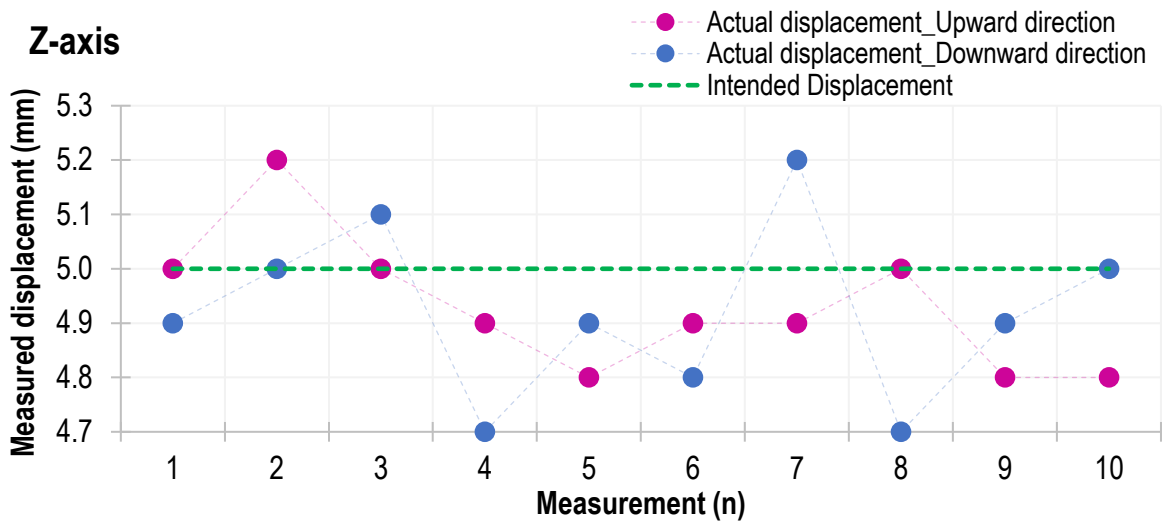

Figure 26: *Actual displacement measured for 5-mm step movement in the Z-axis upward and downward directions versus repetition (n=10). The dotted green line indicates the intended displacement.*

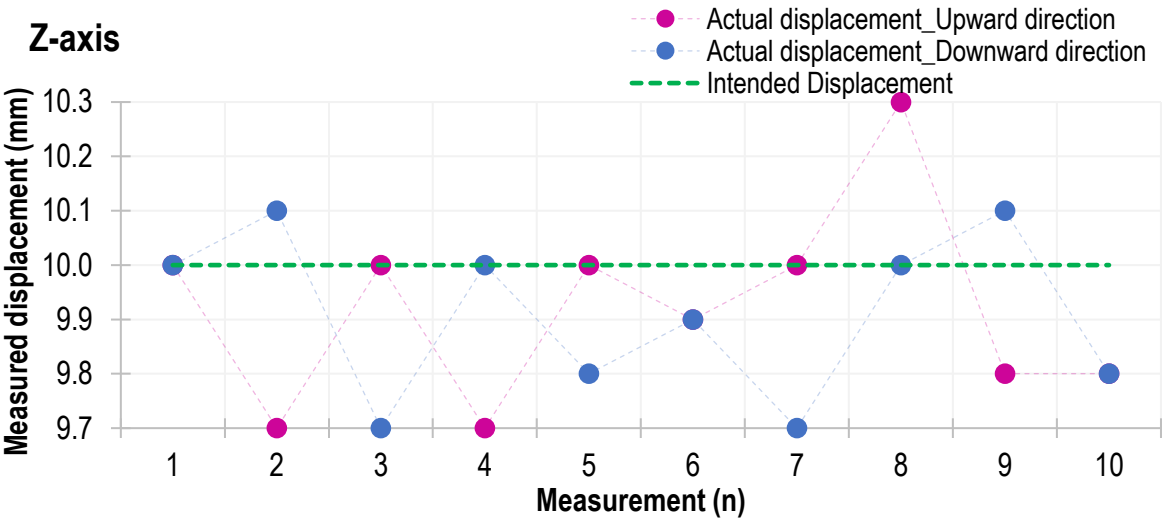

Figure 27: *Actual displacement measured for 10-mm step movement in the Z-axis upward and downward directions versus repetition (n=10). The dotted green line indicates the intended displacement.*

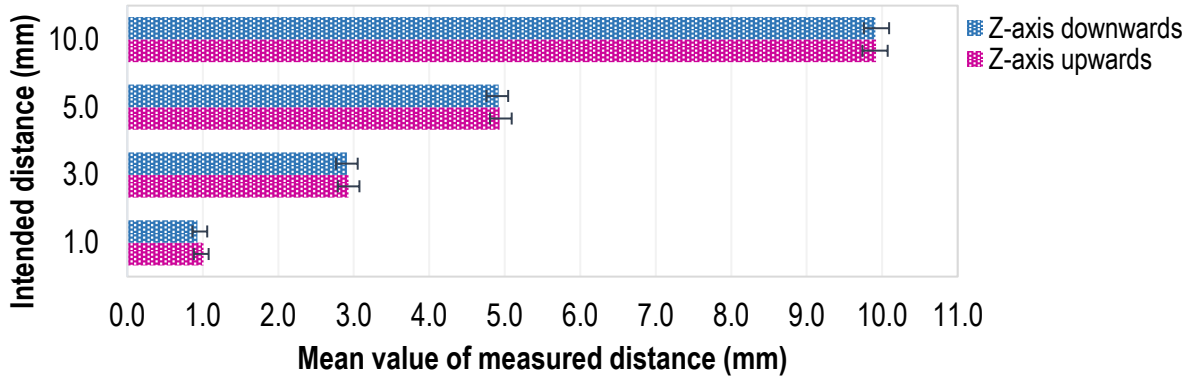

Figure 28*: Intended distance versus mean value of measured distance in the Z-axis upward and downward directions. Error bars represent the standard deviation of the mean.*

2.2.4 Speed of motion

Figure 29 shows the estimated speed of motion in the Y-axis for each repetitive measurement, while also indicating the corresponding mean value and standard deviation.

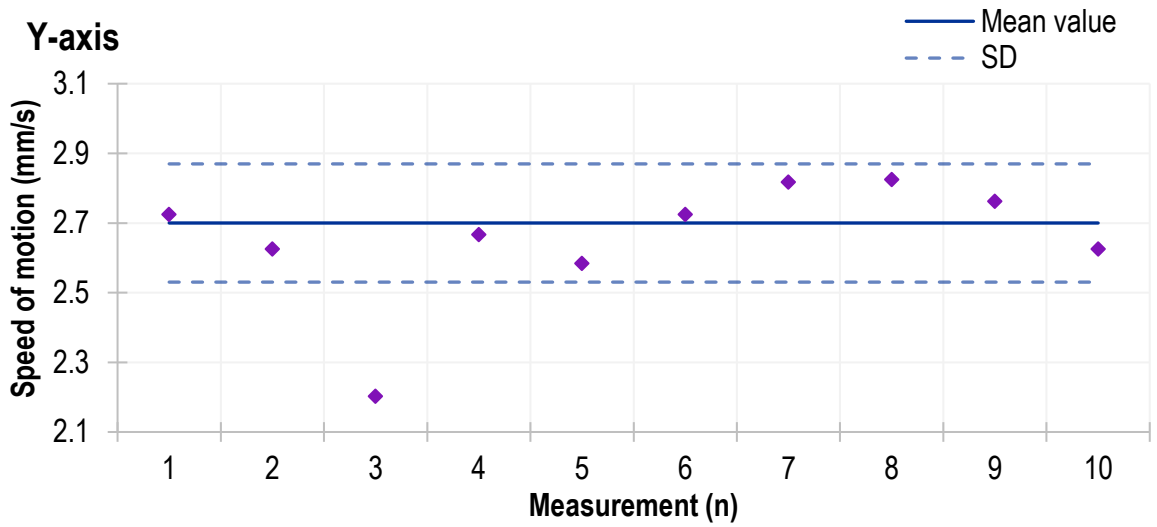

Figure 29: *The estimated motion speed in the Y-axis plotted against measurement number (markers) and the corresponding mean value (solid line). The dotted lines represent the standard deviation (SD) of the mean.*

The graphs of **Figure 30** and **Figure 31** present the relevant results for motion along the X-axis and Z-axis, respectively.

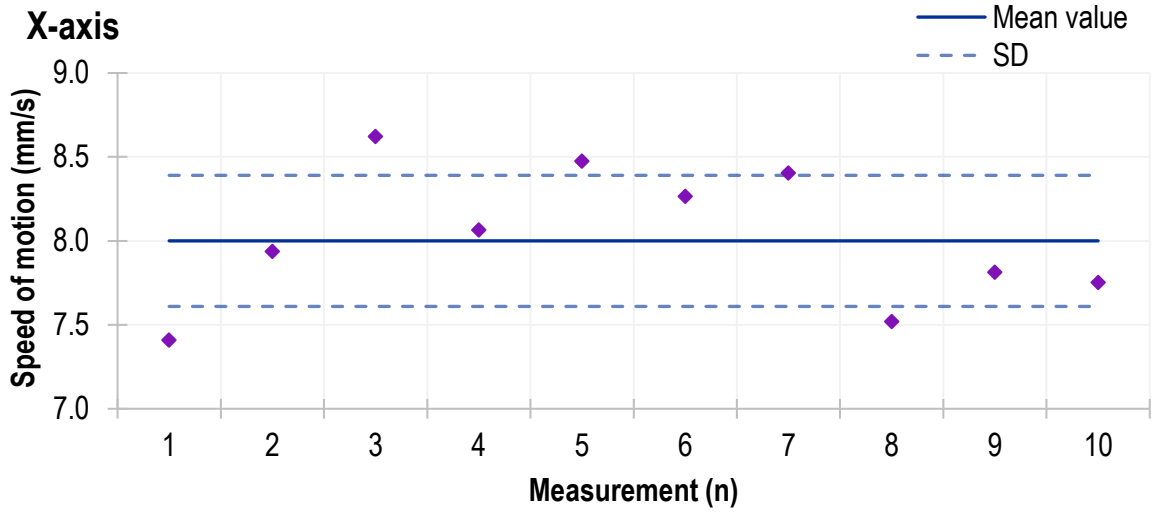

Figure 30*: The estimated motion speed in the X-axis plotted against measurement number (markers) and the corresponding mean value (solid line). The dotted lines represent the standard deviation (SD) of the mean.*

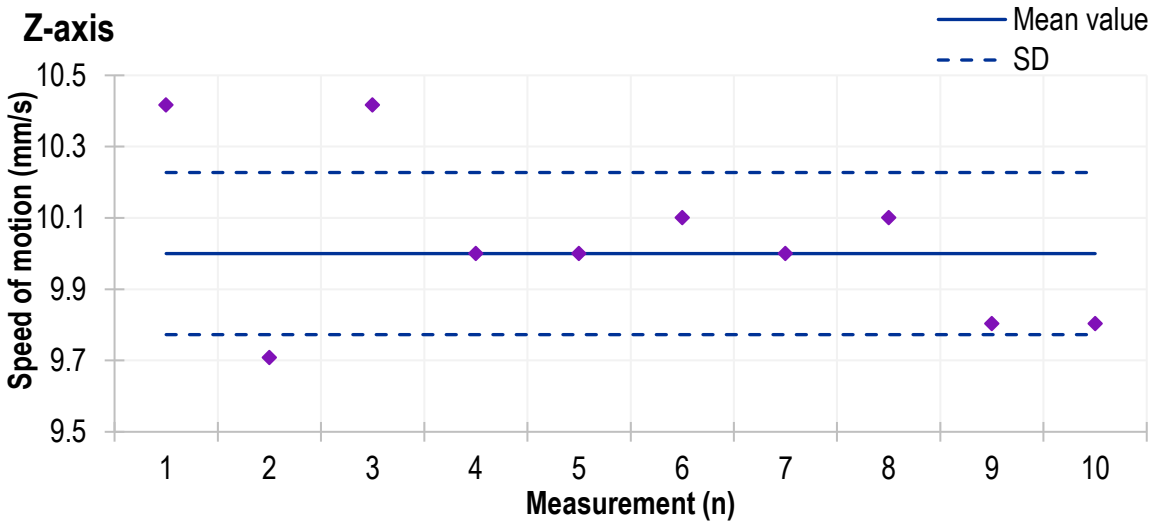

***Figure 31**: The estimated motion speed in the Z-axis plotted against measurement number (markers) and the corresponding mean value (solid line). The dotted lines represent the standard deviation (SD) of the mean.*

2.3 Interpretation of Results

The approach utilized for motion accuracy assessment entailed securing a digital caliper on the evaluated motion stage using custom 3D printed holders, with one end fixed to a stationary section and the other to a movable part of the stage. This arrangement ensured that each step movement of the stage corresponded to a proportional adjustment in the caliper's position. The analysis of motion accuracy demonstrates an average motion error of 0.1 mm, while a maximum motion error of 0.3 mm was observed along all three orthogonal axes (X, Y, Z). The error of the Y-axis forward and reverse motion was almost the same. The same occurred for motion in the X- and Z-axes. Note also that no significant variations in motion accuracy were detected among the stages. Importantly, the small standard deviations of actual displacements (<0.2) calculated from the experimental data suggest excellent repeatability of motion in all linear degrees of freedom.

The speed of linear motion was calculated as well. The activation time of the motors for executing a specific motion command was determined using the Arduino microcontroller and displayed on the software interface. Notably, the motion speed primarily relies on the integrated drivers; nonetheless, the distance of motion remains unaffected by the speed setting parameter of the drivers. The mean motion speed in the X-axis of the robot was estimated at 8.0 ± 0.4 mm/s, while a slightly higher speed of 10.0 ± 0.2 mm/s was estimated in the Z-axis. A significantly smaller speed of 2.7 ± 0.2 mm/s was recorded in the Y-axis. Note that there was no substantial variation in the speed of bidirectional movements (i.e., forward-reverse, right-left, up-down). While excessive speed may compromise the motion accuracy of robotic devices, the increased speed in the X- and Z-axes (compared to the Y-axis) did not affect accuracy.

3. Assessment of motion accuracy in MRI setting

3.1 Materials and Methods

The BRAINSONIC system was integrated with the MRI scanner (3T, Magnetom Vida). The ultrasonic transducer was removed, and a plastic 3D-printed structure was attached to its shaft, serving as the end effector of the mechanism. The structure included a thin tip with a 2-mm diameter, extending towards the acoustic opening of the water contained, which served as a marker on the acquired Fast Low Angle Shot (FLASH) images. The water container was filled with degassed water and the imaging coil (Ultraflex 18 Large, Siemens Healthineers) was positioned at a small distance above utilizing a plastic frame. The setup as arranged on the MRI table is shown in **Figure 32**.

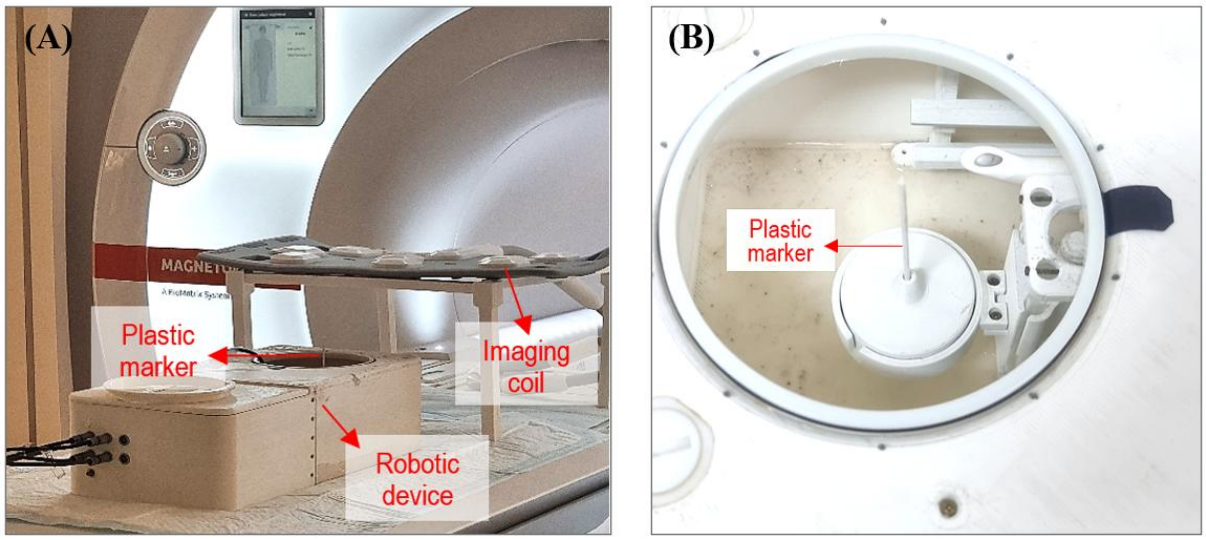

***Figure 32**: (A) Experimental set-up inside the 3 T MRI scanner for motion accuracy assessment. (B) Closer view of the plastic marker as mounted on the mechanism shaft.*

Bidirectional step movements of 3 mm were sequentially performed in each axis to assess the linear motion accuracy of the robotic mechanism. A total of 10 repetitions were performed in each direction. After completion of each 3-mm step, a coronal FLASH image was acquired, revealing the marker's location. **Table 3** lists the imaging parameters utilized for image acquisition.

***Table 3:** Coronal FLASH sequence parameters utilized for motion accuracy assessment.*

Sequence name	**TR (ms)**	**TE (ms)**	**FA (°)**	**NEX**	**Transmit Coil Type**
***fl2d1**	10	3.5	30	10	Body
Slice thickness (mm)	**Matrix**	**pBW (Hz/Pixel)**	**FOV (mm^2)**	**ETL**	**Receive Coil Type**
10	416 x 333	325	140 x 112	1	Ultraflex 18 Large; Spine_72_RS

Following completion of all repetitive step movements, the motion pattern was reconstructed as follows: a) DICOM images were extracted and maintained in their original dimensions before being inserted into Photoshop. b) The MRI grayscale images were converted to black and white to enhance the visibility of the plastic tip - represented as a black spot against a white background. c) The images were superimposed to visualize the motion pattern of the plastic tip.
The corresponding motion errors were calculated through the following steps: a) The Y/X/Z-coordinate of the center of the plastic tip was determined on each DICOM image through the MicroDicom DICOM viewer free software (for assessment in the Y/X/Z axis, respectively). b) The difference in the Y/X/Z-coordinate between adjacent tip locations, i.e., sequential step movements, was calculated. c) The difference was multiplied by the pixel size to determine the shift in mm, indicating the shift in the marker's position along the examined axis.

3.2 Results

Figure 33 displays indicative MRI images obtained for the evaluation of the motion accuracy in the Y-axis right direction. **Figure 34** shows the corresponding images converted into black and white format.

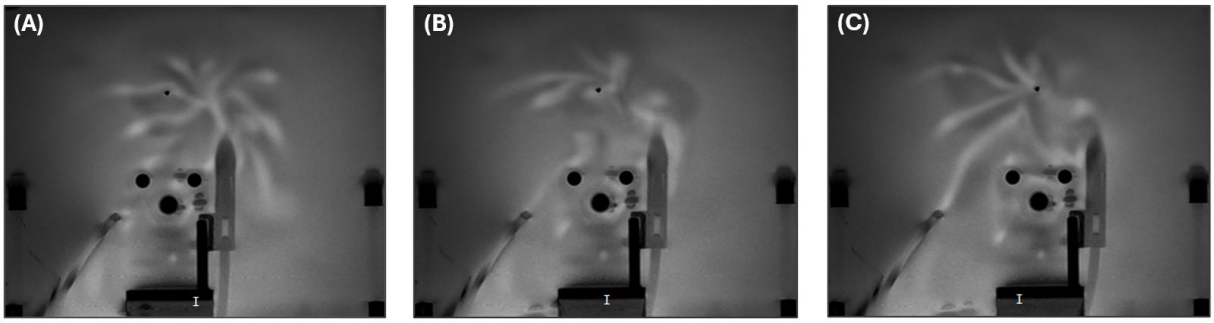

***Figure 33**: Indicative FLASH images acquired after the (A) 1st, (B) 5th, and (C) 10th sequential movements of 3-mm in the Y-axis right direction.*

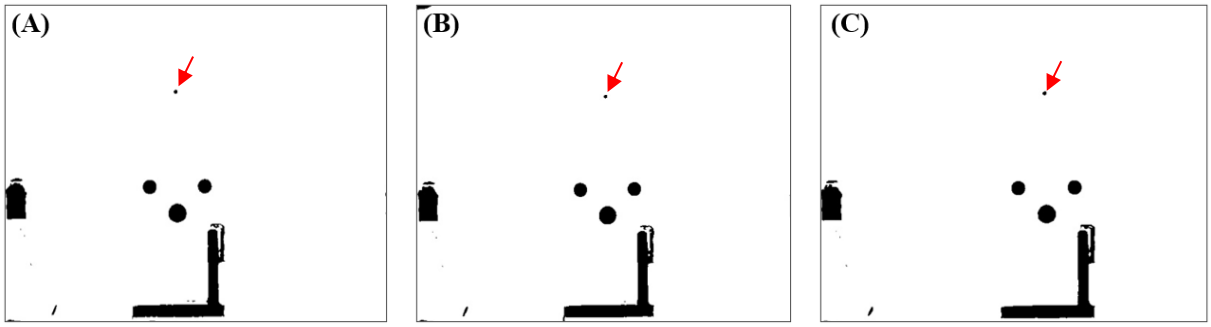

***Figure 34**: Indicative FLASH images acquired after the (A) 1st, (B) 5th, and (C) 10th sequential movements of 3-mm in the Y-axis right direction converted into black and white format.*

The series of (black and white) images were overlaid on one another so that the motion pattern can be visualized, as shown in **Figure 35**, which concerns motion in the right and left directions. Specifically, Figure 35A displays 5 step movements to the left, Figure 35B the subsequent 10 step movements in the opposite direction, and Figure 35C shows the final 5 movements to the left again.

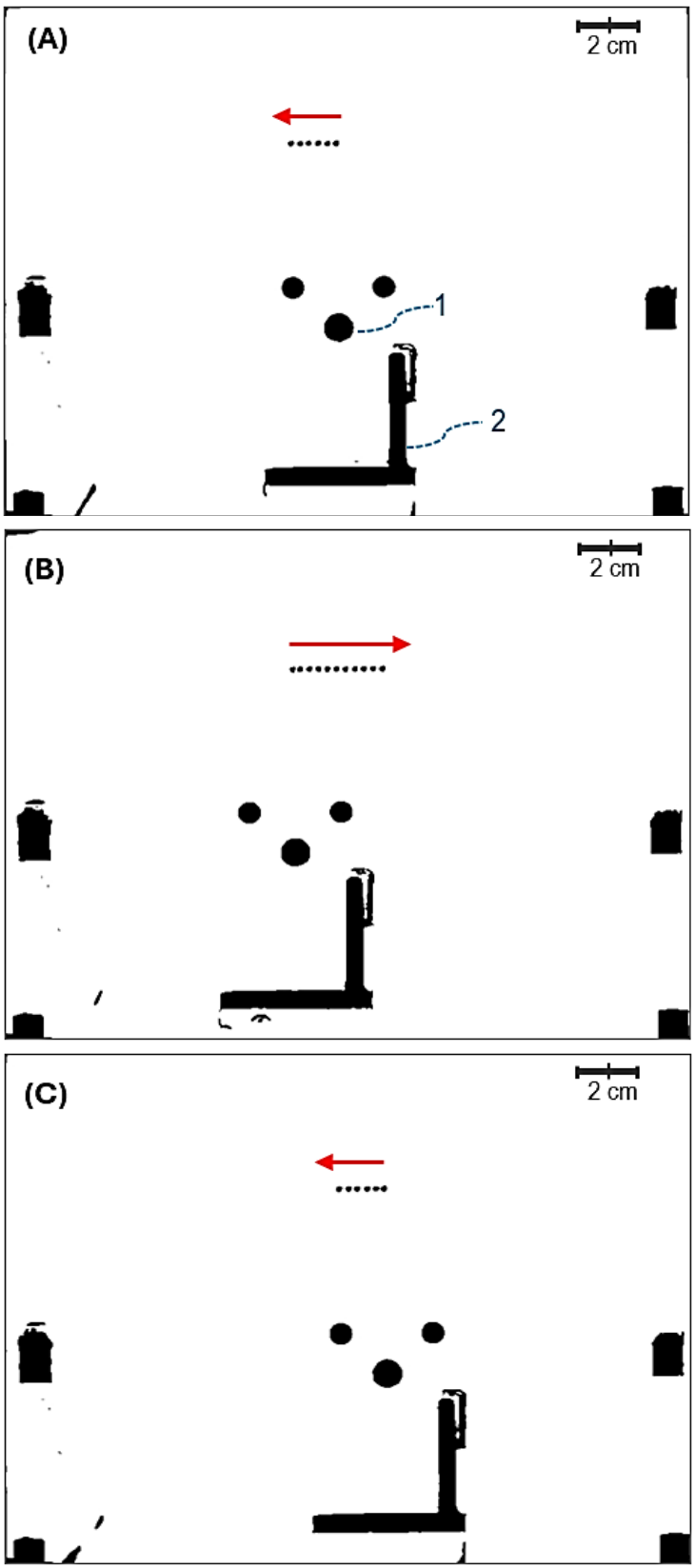

***Figure 35**: Series of acquired FLASH images (converted to black and white format) superimposed onto image, revealing the motion pattern after (A) 5 sequential step movements in the Y-axis left direction, (B) 10 sequential movements in the Y-axis right direction, and (C) 5 movements back to the left direction.*

Table 4 lists the actual (measured) displacement after each step movement in the Y-axis as calculated with the previously described technique. The corresponding mean motion error (different between intended and actual displacement) is also listed in the table.

***Table 4**: List of distance measurements for 3-mm bidirectional step movements in the Y-axis, along with the mean (motion) error and corresponding standard deviation (SD).*

Y-axis direction	Right	Left
Measurement No.	**Measured displacement (mm)**	**Measured displacement (mm)**
1	2.38	2.89
2	3.00	3.20
3	2.99	3.04
4	2.80	2.82
5	2.94	2.82
6	2.76	2.60
7	3.49	2.86
8	2.64	3.44
9	3.24	2.56
10	2.99	3.23
Average	**2.92**	**2.95**
SD	**0.31**	**0.28**
Mean error ± SD (mm)	**0.22 ± 0.21**	**0.24 ± 0.14**

The point charts of **Figure 36** and **Figure 37** show the actual displacement in the MRI setting versus measurement number (repetition) for sequential 3-mm step movements in the Y-axis right and left directions, respectively.

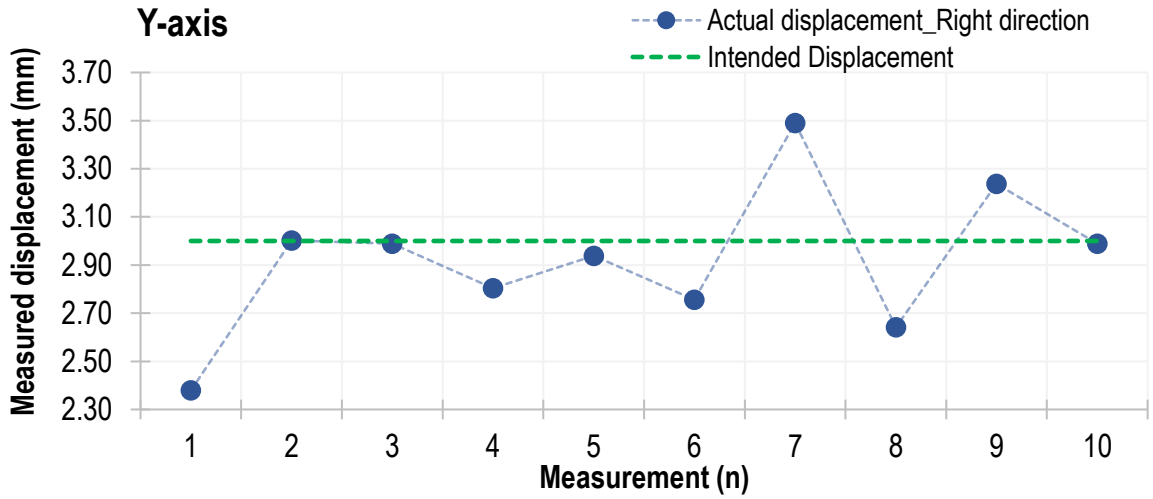

***Figure 36:** Actual displacement measured by MRI for 3-mm step movements in the Y-axis right direction versus repetition (n=10). The dotted green line indicates the intended displacement.*

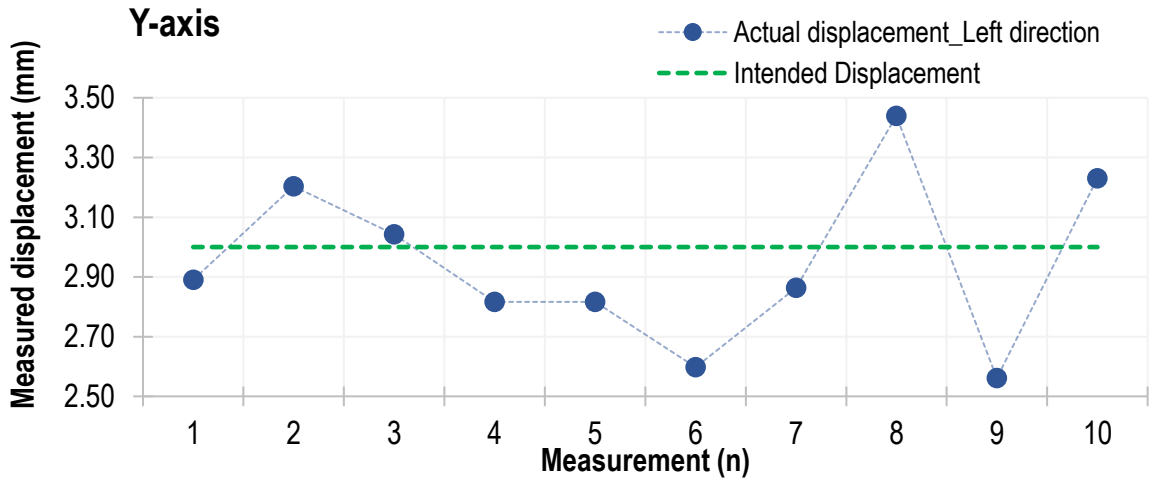

Figure 37: *Actual displacement measured by MRI for 3-mm step movements in the Y-axis left direction versus repetition (n=10). The dotted green line indicates the intended displacement.*

The results of MRI evaluation regarding the accuracy and repeatability of robotic motion for all axes and directions are summarized in **Table 5.**

Table 5*: Mean motion error (± SD) estimated by MRI for all linear motion stages of the robot.*

Axis	Direction	Mean error ± SD (mm)
Y	Right	0.22 ± 0.21
	Left	0.24 ± 0.14
X	Forward	0.21 ± 0.09
	Reverse	0.18 ± 0.13
Z	Upward	0.32 ± 0.17
	Downward	0.30 ± 0.29

3.3 Interpretation of results

Various factors may contribute to inaccuracies in robotic motion within an MRI scanner, including the presence of magnetic interference. Therefore, except from the inherent motion accuracy as determined in a laboratory setting, the accuracy should also be examined within a high field scanner to account for such factors.

A simple and straightforward approach was employed to assess the motion accuracy in the MRI setting. To implement this approach, the ultrasonic transducer was replaced by a 3D-printed plastic structure featuring a 2-mm thick tip, which served as a marker on MRI (FLASH) images. The underlying principle relies on the fact that structures lacking protons appear dark on 'T1-dominant' images. Note that this method is restricted to robotic systems compatible with MRI. The images acquired after repetitive 3-mm step movements in each direction were overlaid onto a single image to visualize the motion patterns, indicating very good repeatability of motion in both directions.

Quantitative analysis suggests that the robot can move with a mean motion error of 0.22 ± 0.21 mm and 0.24 ± 0.14 mm in the right and left directions, respectively. Similar motion error was estimated for the X-axis forward and reverse directions, whereas quite bigger errors were estimated for the Z-axis motion.

CONCLUSIONS

The BRAINSONIC system operated seamlessly within the 3T MRI scanner, experiencing no malfunctions or operational issues. Sufficient SNR for high quality imaging was achieved for both employed sequences (T2-W TSE and SPGR) and maintained among different activations of the robotic system. Notably, coronal imaging yielded significantly higher SNR values compared to axial imaging. Connecting and turning on the electronic system and amplifier had little to no effect on SNR levels, while the most substantial drop occurred upon initiating motion. Visual assessment of the acquired magnitude images revealed no clearly noticeable changes in imaging quality or distortions within the phantom across the different activation states examined.

The accuracy of linear motion was initially assessed in the laboratory through a straightforward methodology, involving the use of a digital caliper. The relevant results substantiate the system's high degree of accuracy and reliability in executing motion tasks. The average motion error was estimated at 0.1 mm across all axes.

Following laboratory validation, the next step was to investigate whether and to what extend MRI affects robotic accuracy. Conducting MRI evaluation is essential to ensure the safe and effective operation of the system in a clinically relevant environment, while accounting for potential sources of error for robots operating within an MRI scanner. The MRI-based method yielded larger motion errors (i.e., lower motion accuracy) in comparison to the benchtop approach. Nevertheless, given the limitations of MRI resolution, the estimated motion errors appear reasonable. Generally, the motion accuracy of the BRAINSONIC system in a 3T scanner remained sufficiently high for reliably delivering ultrasonic energy to the region of interest. Additionally, there was no sign of any mechanical malfunctions, which could compromise the subject’s safety in potential future *in-vivo* trials.